

Theoretical study on $\Xi\alpha$ correlation function

Yuki Kamiya,^{1,2,3,*} Asanosuke Jinno,^{4,†} Tetsuo Hyodo,^{5,2,‡} and Akira Ohnishi^{6,§}

¹*Helmholtz Institut für Strahlen- und Kernphysik and Bethe Center for Theoretical Physics, Universität Bonn, D-53115 Bonn, Germany*

²*RIKEN Interdisciplinary Theoretical and Mathematical Science Program (iTHEMS), Wako 351-0198, Japan*

³*Department of Physics, Tohoku University Sendai 980-8578, Japan*

⁴*Department of Physics, Faculty of Science, Kyoto University, Kyoto 606-8502, Japan*

⁵*Department of Physics, Tokyo Metropolitan University, Hachioji 192-0397, Japan*

⁶*Yukawa Institute for Theoretical Physics, Kyoto University, Kyoto 606-8502, Japan*

(Dated: October 1, 2024)

We study Ξ - ^4He (α) momentum correlation functions in the high-energy nuclear collisions to investigate the nature of the ΞN interactions. We employ the folding $\Xi\alpha$ potential based on the lattice QCD ΞN interactions to compute the correlation function. The $\Xi\alpha$ potential supports a Coulomb-assisted bound state $^5_\Xi\text{H}$ in the $\Xi^-\alpha$ channel, while the $\Xi^0\alpha$ channel is unbound. To examine the sensitivity of the correlation function to the nature of the $\Xi\alpha$ interaction, we vary the potential strength simulating stronger and weaker interactions. The result of the correlation function is sensitive to the existence of the bound state in the $\Xi^0\alpha$ channel, and the characteristic behavior of the bound state remains also in the $\Xi^-\alpha$ correlation with the Coulomb interaction. The effect of the repulsive core of the $\Xi\alpha$ potential can be found in the correlation from the small source as the distinctive dip in the intermediate momentum region.

PACS numbers: 25.75.Gz, 21.30.Fe, 13.75.Ev

I. INTRODUCTION

Understanding the properties of the Hyperon (Y)-Nucleon (N) interactions is a long standing problem in the hypernuclear physics. Among others, the ΞN interaction in the strangeness $S = -2$ sector is important to pin down the role of Ξ in the neutron star and possible existence of the H dibaryon [1]. There are four independent components in the s -wave ΞN interaction, $^{11}S_0$, $^{31}S_0$, $^{13}S_1$, $^{33}S_1$ where the notation $^{2I+1,2s+1}L_J$ is adopted with the spin s , isospin I , and the total angular momentum J .

Through the recent experimental observations of the Ξ hypernuclei [2–4], the ΞN interaction is considered to be moderately attractive in total. This is consistent with the recent theoretical analysis with the chiral effective field theories [5–7] and the lattice QCD calculations [8, 9]. On the other hand, the scattered results of the theoretical predication on the light Ξ hypernuclei [10–17] indicate that the detailed understanding of the ΞN interactions is still insufficient and further constraints through the experimental observables are required.

In the past few years, the femtoscopic study using the momentum correlation function from the high-energy collisions provides new insights for the hyperon interactions. The correlation function is known to be sensitive to the low-energy interaction and the particle emission source. In addition, the femtосopy approach is advantageous for the multi-strangeness sector which is not easily studied by the traditional scattering experiments. For the baryon pairs including strangeness, $p\Lambda$ [18–20], $p\Sigma^0$ [21], $p\Xi^-$ [22–24] $\Lambda\Lambda$ [19, 24–26], $\Lambda\Xi$ [27], $\Xi\Xi$ [24] and $p\Omega$ [23, 28] correlation data have

been reported experimentally.

For the study of the ΞN interactions, $p\Xi^-$ correlation functions from the pp [23] and $p\text{Pb}$ collisions [22] are measured by the ALICE collaboration. The corresponding theoretical studies can be found in Refs. [29–32]. In Ref. [30], the ALICE data are shown to be consistent with the theoretical correlation function calculated with the lattice QCD ΞN - $\Lambda\Lambda$ coupled-channel potential [9]. The measured correlation function is also in good agreement with the results in Refs. [29, 31, 32], which are evaluated with the chiral effective field theory [5, 7], although the spin-isospin components of the ΞN interaction exhibit different properties from the lattice QCD potential. This is because the enhancement of the ΞN correlation is originated mainly in the strong attraction in the $^{11}S_0$ component, which shows similar behavior in both potentials. Thus, with these studies, strongly attractive nature of the $^{11}S_0$ interaction is well confirmed, while the other components still lack the thorough understanding.

To impose further constraints on the ΞN interaction by the femtoscopic study, it is interesting to consider the correlation between Ξ and nuclei. The correlation functions including nuclei have recently been studied theoretically [33–40] and experimentally [41, 42]. Because the Ξ -nucleus correlation picks up different combination of the spin-isospin components from the $p\Xi^-$ correlation function, further constraints on the ΞN interactions can be imposed by the study of the Ξ -nucleus correlation. In this direction, the deuteron- Ξ correlation is studied in Ref. [37], and it is found that the clear enhancement by the strong interaction appears in the correlation function, while the deuteron breakup effect is sufficiently weak. However, in general, complicated three-body dynamics plays an important role in the correlation with the weakly bound deuteron [38].

Another possible candidate for the femtосopy is the pair of a hyperon and ^4He (α) particle. The tightly bound nature of α justifies the two-body treatment of the hyperon- α

* yuki.kamiya.d3@tohoku.ac.jp

† jinno.asanosuke.36w@st.kyoto-u.ac.jp

‡ hyodo@tmu.ac.jp

§ Deceased.

system. In fact, a recent theoretical study of the $\Lambda\alpha$ correlation function shows that the femtoscopic analysis of $\Lambda\alpha$ helps to investigate the ΛN interaction [39]. It is also found that the $\Lambda\alpha$ correlation function exhibits unique feature not seen in the hadron-hadron correlation functions, due to the relatively longer interaction range of the hyperon-nucleus interaction [39]. In addition, the $\Xi\alpha$ correlation can be used to disentangle the various spin-isospin components of the ΞN interaction. The $\Xi\alpha$ interaction is expressed by the weighted sum of the ΞN interaction components as $[V(^{11}S_0) + 3V(^{31}S_0) + 3V(^{13}S_1) + 9V(^{33}S_1)]/16$. Namely, the $\Xi\alpha$ interaction is dominated by the $^{33}S_1$ component of the ΞN interaction [16]. Thus the $\Xi\alpha$ correlation brings the information complementary to the $p\Xi^-$ correlation.

There are two charge channels, $\Xi^0\alpha$ and $\Xi^-\alpha$; the former is governed solely by the strong interaction, while additional attraction is given to the latter by the Coulomb interaction. The theoretical studies of the Ξ hypernuclei [13, 16] predict the existence of a shallow bound state $^5_{\Xi}\text{H}$ in the $\Xi^-\alpha$ channel but no bound state in the $\Xi^0\alpha$ channel. Such a shallow bound state that vanishes when the Coulomb interaction is switched off is called Coulomb-assisted bound state. The binding energy of $^5_{\Xi}\text{H}$ depends on the employed ΞN interactions, mainly due to the difference in the $^{33}S_1$ component which gives the largest contribution [13]. Because it is known that the correlation function is sensitive to the existence and the binding energy of the bound state [43, 44], the $\Xi\alpha$ correlation function is expected to be helpful to elucidate the nature of the $^5_{\Xi}\text{H}$ state and the $\Xi\alpha$ interaction. However, it is unknown how the correlation functions of the charged pair behave when the Coulomb-assisted bound state emerges.

In this study, we give theoretical predictions for the $\Xi\alpha$ correlation function which can be measured in future experiments. We employ the $\Xi\alpha$ folding potential [16] constructed with the HAL QCD ΞN interactions [9]. To consider the theoretical uncertainties, we vary the strength of the potential to realize the case with and without the $\Xi\alpha$ bound state, and see how the correlation is affected by the variation of the potential strength. Furthermore, to investigate the relevance of the detailed shape of the interaction potential, we prepare the simple Gaussian potential models and compare the results with those by the folding potentials.

This article is organized as follows. In Sec. II, we briefly review the current status of the $\Xi\alpha$ interactions and introduce the framework to calculate the $\Xi\alpha$ correlation function. In Sec. III, we show the results of the $\Xi\alpha$ correlation functions with examining various potentials and approximations. Section IV is devoted to a summary and concluding remarks.

II. FORMALISM

In this study, we treat the $\Xi\alpha$ pair as a two-body system of Ξ and α , without considering the α breakup processes. We employ the $\Xi\alpha$ folding potential developed in Ref. [16]. The folding potential is constructed by using the HAL QCD ΞN potentials [9] where the small ΞN - $\Lambda\Lambda$ coupling in the $^{11}S_0$ channel is renormalized into the effective single channel ΞN

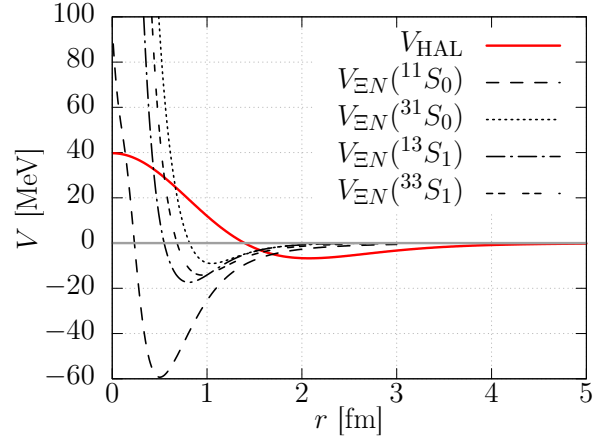


FIG. 1. The $\Xi\alpha$ folding potential V_{HAL} [16] and the HAL QCD ΞN potentials $V_{\Xi N}(^{2I+1, 2S+1}L_J)$ [9]. For $V_{\Xi N}$, the central values of $t = 12$ data are plotted.

potential with a real coupling strength. This folding $\Xi\alpha$ potential is parametrized by the sum of the Gaussians as

$$V_{\text{HAL}}(r) = \sum_{i=1}^{20} V_i \exp(-\nu_i r^2), \quad (1)$$

where V_i is the potential strength and ν_i is the Gaussian range. Because the tiny decay process $\Xi N \rightarrow \Lambda\Lambda$ is not included in the construction, V_i are the real parameters. The shape of the $\Xi\alpha$ folding potential is shown in Fig. 1 together with the HAL QCD ΞN potentials. It is seen that the potential V_{HAL} has a repulsive core at short distance and an attractive pocket in the longer range, as in the ΞN interactions. Due to the spatial extent of the α particle, both the central repulsion and the attractive pocket are smeared from the ΞN interactions. As a consequence, the range of the $\Xi\alpha$ potential is longer than the ΞN interactions. By solving the Schrödinger equation, the attraction of V_{HAL} turns out to be not strong enough to support a bound state.

In the practical calculations, we need to consider the $\Xi^0\alpha$ and $\Xi^-\alpha$ systems separately, due to the Coulomb interaction. The $\Xi^0\alpha$ system, where only the strong interaction works, does not have a bound state. The scattering length a_0 and the effective range r_e are summarized in Table I. Note that we employ the nuclear physics convention for the scattering length where positive (negative) a_0 corresponds to the repulsive interaction or the strongly attractive interaction with a bound state (weakly attractive interaction without a bound state). This significantly large scattering length $|a_0| \sim 500$ fm implies that the system is very close to the unitary limit [45] and the bound state would appear if the attraction were slightly stronger. The larger effective range r_e than usual hadron potentials reflects the longer interaction range of the $\Xi\alpha$ potential (1).

For the $\Xi^-\alpha$ system, the further attraction by the Coulomb

TABLE I. The scattering length a_0 and the effective range r_e of the $\Xi^0\alpha$ scattering calculated with the folding potential V_{HAL} and its variations V_{strong} and V_{weak} .

potential	a_0 [fm]	r_e [fm]
V_{HAL}	-522.8	4.50
$V_{\text{strong}} = 2V_{\text{HAL}}$	6.39	3.01
$V_{\text{weak}} = V_{\text{HAL}}/2$	-3.39	7.36

interaction acts as

$$V_{\text{Coulomb}}(r) = -\frac{2\alpha}{r}, \quad (2)$$

with the fine structure constant α . By solving the Schrödinger equation with $V = V_{\text{HAL}} + V_{\text{Coulomb}}$, we find a Coulomb-assisted shallow bound state $\Xi^5\text{H}$ with the binding energy

$$B = 0.47 \text{ MeV}. \quad (3)$$

Note that this is distinguishable from the Coulomb bound states, which emerge from the purely Coulombic attraction. The binding energy of the ground state by the pure Coulomb potential is given as

$$B^{\text{Coulomb}} = \frac{\alpha}{a^{\text{Bohr}}} = 0.104 \text{ MeV}, \quad (4)$$

with the Bohr radius of the $\Xi^-\alpha$ system $a^{\text{Bohr}} = (2\mu_{\Xi^-\alpha})^{-1} = 13.9 \text{ fm}$. Compared with B^{Coulomb} , the binding energy $B = 0.47 \text{ MeV}$ is about 0.3 MeV deeper and its dominant contribution should come from the strong interaction V_{HAL} .¹

In the study of chiral effective field theory [13], the $\Xi^5\text{H}$ bound state with $B = 2.16 \text{ MeV}$ is found by using the chiral next-to-leading order (NLO) ΞN interactions. This indicates that the chiral $\Xi\alpha$ interaction is more attractive than the HAL QCD based potential V_{HAL} . On the other hand, because the strength of the $\Xi\alpha$ potential is to some extent ambiguous, the $\Xi\alpha$ potential might be less attractive than V_{HAL} without generating the bound $\Xi^5\text{H}$. To examine the theoretical uncertainty of the $\Xi\alpha$ potential, we consider two variations of the potential; $V_{\text{strong}} = 2V_{\text{HAL}}$ and $V_{\text{weak}} = V_{\text{HAL}}/2$ for the stronger and weaker potentials, respectively. These variations are shown in Fig. 2. With the stronger potential V_{strong} , the $\Xi^5\text{H}$ binding energy is found to be 2.08 MeV, which is close to the value in the chiral NLO analysis. In addition, this stronger potential V_{strong} makes a bound state also in the $\Xi^0\alpha$ channel without the Coulomb attraction. Accordingly, the scattering length a_0 becomes positive. On the other hand, the binding energy of $\Xi^5\text{H}$ with the weaker potential V_{weak} is 0.18 MeV, which is of the same order with the binding energy of the Coulomb bound state (4). As expected, there is no bound state in the $\Xi^0\alpha$ system with V_{weak} . The scattering lengths a_0 , effective ranges

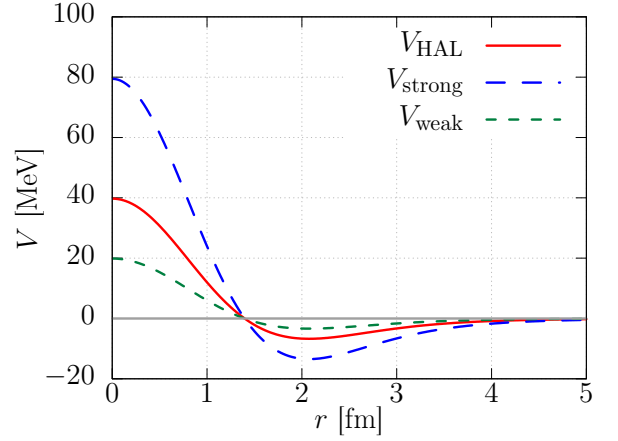


FIG. 2. Comparison of the $\Xi\alpha$ folding potential V_{HAL} and its variations of V_{strong} and V_{weak} .

TABLE II. The binding energy of the $\Xi^-\alpha$ and $\Xi^0\alpha$ systems. The Coulomb interaction is included in the $\Xi^-\alpha$ calculation.

potential	$\Xi^-\alpha$ [MeV]	$\Xi^0\alpha$ [MeV]
V_{HAL}	0.47	-
V_{strong}	2.08	1.15
V_{weak}	0.18	-

r_e , and the binding energies of the $\Xi\alpha$ systems for different potentials are summarized in Table I and II.

In the present framework, the $\Xi\alpha$ system is treated as a single-channel scattering. For a given $\Xi\alpha$ potential, the momentum correlation function $C(\mathbf{q})$ in the high-energy nuclear collisions can be calculated by the Koonin-Pratt (KP) formula [46–49];

$$C(\mathbf{q}) = \int d^3r S(\mathbf{r}) \left| \Psi^{(-)}(\mathbf{q}; \mathbf{r}) \right|^2, \quad (5)$$

where \mathbf{q} is the relative momentum in the pair rest frame, $S(\mathbf{r})$ is the normalized source function, and $\Psi^{(-)}(\mathbf{q}; \mathbf{r})$ is the relative wave function with the outgoing boundary condition, calculated by the potential. In this study, we employ the static Gaussian source function $S_R(r) \equiv \exp(-r^2/4R^2)/(4\pi R^2)^{3/2}$ with the source size² R . For the $\Xi^0\alpha$ pair, we consider the modification of the wave function from the plane wave only in the s -wave component, which is significantly distorted by the strong interaction in the low-momentum region. On the other hand, for the $\Xi^-\alpha$ pair, because of the long range nature of the Coulomb interaction, one

¹ For the detailed discussion on the contribution of the Coulomb potential on the bound states, see Appendix A.

² We note that $S(r)$ is the relative source function representing the distribution of the $\Xi\alpha$ pair emitted with the relative distance r . The relative source size is defined as $R = \sqrt{(R_\Xi^2 + R_\alpha^2)/2}$ with R_Ξ (R_α) being the source size of the single Ξ (α) production. With this definition, the relative source is given by the gaussian with radius $\sqrt{2}R$ [49].

must use the Coulomb wave functions as the asymptotic form in all the partial waves, and introduce the strong interaction effect in the s wave [50].

III. RESULTS

First we discuss the $\Xi^0\alpha$ correlation function without the Coulomb attraction. The results with V_{HAL} , V_{strong} , and V_{weak} for $R = 1, 3$, and 5 fm are shown in Fig. 3.³ We see that $C_{\Xi\alpha}$ with V_{strong} shows qualitatively different behavior from those with V_{HAL} and V_{weak} . This is attributed to the existence of the bound state by V_{strong} . In addition, the very strong enhancement of the correlation with V_{HAL} at small momentum reflects the significantly large scattering length $|a_0| > 500$ fm. As a consequence, three different potential models adopted here are distinguishable by the measurement of the $\Xi^0\alpha$ correlation function, in particular for the large source $R = 3$ – 5 fm. We find that the result with V_{strong} shows the suppression or bump structure depending on the source size R . This is a typical feature of $C_{\Xi\alpha}$ for the attractive interaction with a bound state. On the other hand, the correlation functions with V_{HAL} and V_{weak} show the enhancement in the low momentum region characteristic for an attractive interaction without a bound state, but a dip structure in the intermediate momentum region ($q \sim 200$ MeV/c) is found. The dip structure is more prominent in $C_{\Xi\alpha}$ with a small source, $R = 1$ fm. Because such dip structure is not seen in the model calculation with simple attraction [53], this should be related to the detailed shape of the $\Xi\alpha$ potential.

To see the effect of the shape of the $\Xi\alpha$ folding potential, we introduce the purely attractive one range Gaussian potential given as

$$V_{\text{Gaussian}}(r) = V_0 \exp(-r^2/b^2), \quad (6)$$

with the potential strength V_0 and the range parameter b . We construct the Gaussian potentials by choosing the range parameter as $b = 3$ fm and tuning V_0 to reproduce the scattering length a_0 in Table I for each potential. We have checked that the qualitative conclusions given below remain unchanged under the variation of the value of b . The correlation functions by the Gaussian potentials with $R = 1$ fm are compared with the results from the original folding potentials V_{HAL} , V_{strong} , and V_{weak} in Fig. 4. We find that the Gaussian potentials qualitatively reproduce the results of the original folding potentials, while the correlation in the small momentum region is somewhat overestimated. In particular, the Gaussian potentials corresponding to V_{HAL} and V_{weak} without a bound state provide the enhancement of the correlation without a dip in the intermediate momentum region, as expected. In other words, the

folding potentials with a repulsive core gives the suppression of the correlation functions in this region, causing a dip structure. Thus, we conclude that the characteristic suppression found in the $\Xi^0\alpha$ correlation with $R = 1$ fm in the intermediate momentum region is caused by the repulsive core of the folding potential. This means that the correlation function from the small source may be useful to investigate the existence and strength of the repulsive core of the $\Xi\alpha$ interaction.

To further discuss the effect of the potential shape to the correlation, we evaluate the correlation functions with the Lednicky-Lyuboshits (LL) formula [49, 54]

$$C_{\text{LL}}(q) = 1 + \frac{|f(q)|^2}{2R^2} F_3\left(\frac{r_{\text{eff}}}{R}\right) + \frac{2\text{Re}f(q)}{\sqrt{\pi}R} F_1(2qR) - \frac{\text{Im}f(q)}{R} F_2(2qR), \quad (7)$$

where $F_1(x) = \int_0^x dt e^{t^2-x^2}/x$, $F_2(x) = (1 - e^{-x^2})/x$, $F_3(x) = 1 - x/2\sqrt{\pi}$, and $f(q) = 1/(-1/a_0 + r_e/2q^2 - iq)$ is the s -wave $\Xi\alpha$ scattering amplitude calculated by the effective range expansion with the threshold parameters in Table I. The LL formula is obtained from the KP formula by approximating the full wave function by the asymptotic wave function. This means that if the detailed shape of the potential affects the correlation function, the LL formula estimation should be deviated from the result of the KP formula. In Fig. 4, we compare the results by the KP formula (5) with the corresponding ones by the LL formula for V_{HAL} , V_{strong} , and V_{weak} potentials with the source size $R = 1$ fm. As shown in Fig. 4, for $R = 1$ fm case, the results with the LL formula do not reproduce those with the KP formula for all potentials. In particular, in the low momentum region, C_{LL} rapidly decreases, while the result of the KP formula shows the strong enhancement. Note that $C_{\Xi\alpha}$ defined in Eq. (5) is always positive while C_{LL} can be negative in the small momentum region when r_e is large and positive. The negative C_{LL} seen in Fig. 4 also indicates that the LL formula is not applicable in these cases. On the other hand, as shown in Fig. 5 for $R = 3$ fm and $R = 5$ fm cases, the LL formula gives the good approximation of the KP formula results. This is because the correlation from the large source is determined mainly by the distortion of the wave function at large relative distance r where the detailed potential shape is irrelevant. This failure of the LL formula for small source is qualitatively consistent with what is found in the study of the $\Lambda\alpha$ correlation function [39].

Finally, we show the results of the $\Xi^-\alpha$ correlation functions in Fig. 6. Due to the Coulomb attraction, $C_{\Xi\alpha}$ shows the strong enhancement at the low momentum for all potentials. The effect of the strong interaction emerges as the deviation from the pure Coulomb result, where the strong interaction is switched off. In contrast to the $\Xi^0\alpha$ correlation, the difference between the adopted potentials in larger source is smeared by the Coulomb attraction. Nevertheless, with a good resolution of the measurement, it may be possible to distinguish different potentials by the correlation function with $R = 1$ – 3 fm. Through the comparison with $C_{\Xi^0\alpha}$ in Fig. 3, we find that the results with V_{strong} and V_{weak} in the low momentum region is simply enhanced due to Coulomb force from $C_{\Xi^0\alpha}$. On the

³ The source size $R = 1$ fm might look small for the emission of the α particle with the charge radius ~ 1.68 fm [51]. As we mentioned, however, the relative source function $S(r)$ has the gaussian width $\sqrt{2}R$, and the probability distribution of the relative distance r is given by $4\pi r^2 S(r)$ [52]. As a consequence, with $R = 1$ fm, the mean distance between the emitted pair is about $\langle r \rangle = 4R/\sqrt{\pi} \sim 2.26$ fm.

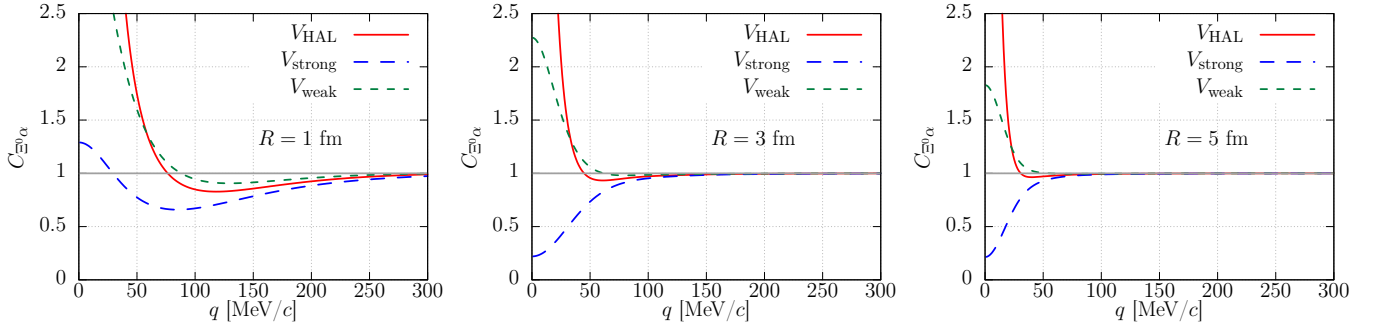


FIG. 3. The $\Xi^0\alpha$ correlation function with $R = 1, 3$, and 5 fm. The results with V_{HAL} , V_{strong} , and V_{weak} are shown by solid, long-dashed, and dashed lines respectively.

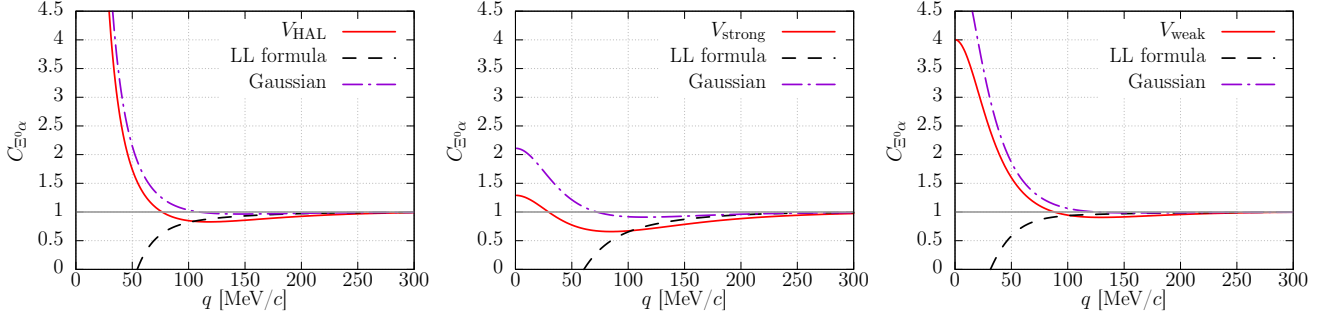


FIG. 4. Comparison of $\Xi^0\alpha$ correlation functions for $R = 1$ fm with the KP formula for the folding potential (solid lines), the Gaussian potential model (dash-dotted lines), and the LL formula estimation (dashed lines). The left, central, and right panel show the results with V_{HAL} , V_{strong} , and V_{weak} , respectively.

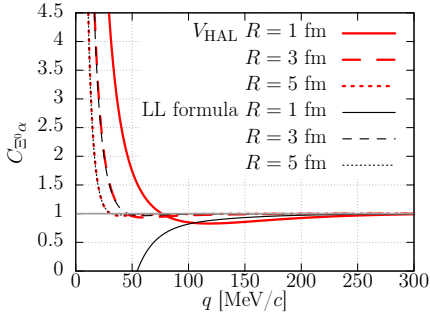


FIG. 5. Comparison of $\Xi^0\alpha$ correlation functions by V_{HAL} with the KP formula (thick lines) and the LL formula estimation (thin lines) for different source sizes. The results with $R = 1, 3$, and 5 fm are denoted by solid, dashed, and dotted lines, respectively.

other hand, $C_{\Xi^-\alpha}$ with V_{HAL} with $R = 3$ and 5 fm is smaller than the pure Coulomb case while $C_{\Xi^0\alpha}$ shows the enhancement. Namely, the correlation function of V_{HAL} shows enhancement for the small source and suppression for the large source with respect to the pure Coulomb result. This is nothing but the source size dependence of the correlation function with a shallow bound state. This means that, when the Coulomb-assisted bound state exists, the typical source size

dependence can be observed in the $\Xi^-\alpha$ correlation function as the difference from the pure Coulomb result.

IV. CONCLUSION

Towards elucidating the ΞN interaction, we have discussed the $\Xi\alpha$ correlation function with the folding potential V_{HAL} [16] obtained with the latest ΞN lattice QCD interactions [9], which give the large scattering length without a bound state (a shallow Coulomb-assisted bound state) in the $\Xi^0\alpha$ ($\Xi^-\alpha$) channel. Two variants of the $\Xi\alpha$ potential, V_{strong} and V_{weak} , are used to discuss the dependence on the binding energy and existence of the bound states for the correlation function. The $\Xi^0\alpha$ correlations with V_{strong} for the source sizes $R = 1, 3$, and 5 fm show the source size dependence typical to the system with a bound state. On the other hand, the correlations with V_{HAL} and V_{weak} exhibit the characteristic suppression in the intermediate momentum region on top of the strong enhancement typical to the system with attractive interactions without a bound state.

To discuss the effect of the shape of the $\Xi\alpha$ potential on the correlation function, the results with the folding potentials are compared with those by the purely attractive Gaussian potential model and by the LL formula. The LL results do not reproduce the folding potential for the small source

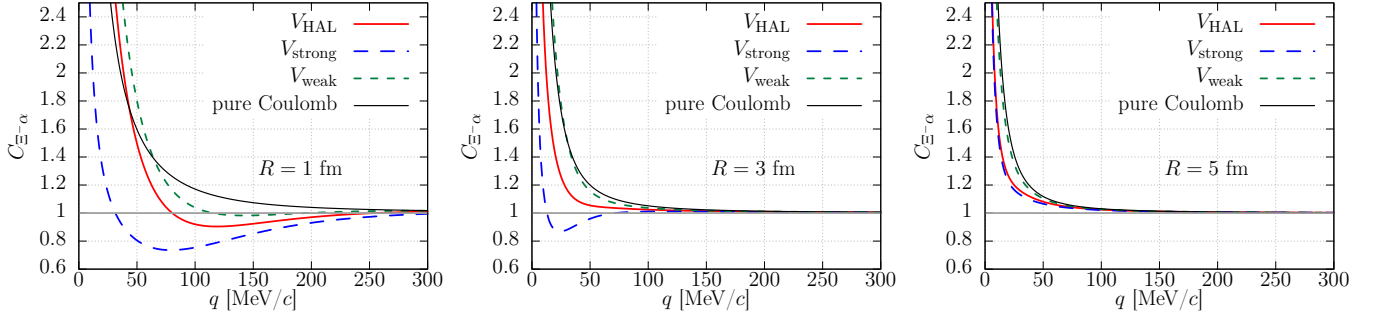


FIG. 6. The $\Xi^- \alpha$ correlation function with $R = 1, 3$ and 5 fm. The results with V_{HAL} , V_{strong} , and V_{weak} are shown by solid, long-dashed, and dashed lines respectively. The pure Coulomb result, where the strong interaction is switched off, is shown by the solid thin line for comparison.

cases, indicating that the correlation function is sensitive to the detailed shape of the potential. Because the dip structure in the intermediate momentum region is not seen in the Gaussian potential result, we conclude that the central repulsion of the folding potential is the origin of the suppression causing the dip. Thus, the strength of the central repulsion of the $\Xi \alpha$ potential is reflected in the dip structure found in the intermediate momentum region.

The $\Xi^- \alpha$ correlation with V_{HAL} shows the source size dependence reflecting the emergence of the ${}^5_{\Xi} \text{H}$ state. This result ensures that the strength of the $\Xi \alpha$ attraction, which originates in the ΞN interaction, and the existence of the Coulomb-assisted bound state of ${}^5_{\Xi} \text{H}$ can be investigated by the source size dependence of the $\Xi^- \alpha$ correlation.

In this study, we take the source sizes $R = 1, 3$, and 5 fm for the theoretical prediction for the small to large source experiments. These values correspond to the typical sizes used in the analysis of the two-hadron correlation functions obtained in the high-energy pp and heavy ion collisions. However, the effective source size of the composite particle α , which can also be formed by the coalescence of four nucleons emitted from the fireball, must be larger than those with single hadron emissions [33–35]. In fact, the $\Xi \alpha$ pair is treated as a pair of the point-like particles in the Koonin-Pratt formula (5), which gives the normalization of the emitting source function. For a more realistic study of the $\Xi \alpha$ correlation, the five body scattering problem of four nucleons and alpha should be solved to take into account the coalescence effect, which is left as future works.

We have shown that the difference of the correlation functions from different $\Xi \alpha$ potentials, V_{HAL} , V_{strong} , and V_{weak} can be well distinguished by the measurement of the $\Xi \alpha$ correlation functions, in particular by those from $R \sim 3$ fm source. To measure the $\Xi \alpha$ correlation in experiments, it is desirable to use the high-energy collisions with the central energy $\sqrt{s_{NN}} < 10$ GeV, where a bunch of α is produced according to the estimation in Ref. [55]. For this reason, it is anticipated that the $\Xi \alpha$ correlation can be experimentally measured in the facilities such as FAIR [56], NICA, and J-PARC-HI [57] to elucidate the $\Xi \alpha$ interaction and its origin of the ΞN interactions.

ACKNOWLEDGMENTS

We thank Emiko Hiyama for providing the $\Xi \alpha$ folding potential and for the helpful support. We also thank Kouichi Hagino, Yudai Ichikawa, Johann Haidenbauer, Andreas Nogga, Hoai Le, and Avraham Gal for useful discussions and comments. This work was supported in part by the Grants-in-Aid for Scientific Research from JSPSs (Grants No. JP23H05439, and No. JP22K03637), by JST, the establishment of university fellowships towards the creation of science technology innovation, Grant No. JPMJFS2123, by JST SPRING, Grant Number JPMJSP2110, and by the Deutsche Forschungsgemeinschaft (DFG) and the National Natural Science Foundation of China (NSFC) through the funds provided to the Sino-German Collaborative Research Center “Symmetries and the Emergence of Structure in QCD” (NSFC Grant No. 12070131001, DFG Project-ID 196253076 – TRR 110).

Appendix A: Contribution of the Coulomb potential on bound states

In this appendix, we discuss the effect of the Coulomb potential on the $\Xi^- \alpha$ bound states. Because the attractive Coulomb force always supports infinitely many bound states, it is difficult to distinguish whether the bound state by the Coulomb plus short range interaction originates mainly from the Coulomb interaction or from the strong interaction when the binding energy B is comparable with the ground state energy by the pure Coulomb force B^{Coulomb} (4). One way to quantify the effect of the Coulomb potential is to evaluate the spatial extent of the bound state wave function. In Fig. 7, we show the ground state wave functions ψ_{bound} by Coulomb plus V_{HAL} , V_{weak} , V_{strong} and the pure Coulomb potentials. ψ_{bound} with pure V_{Coulomb} has the long range tail, which is also found in ψ_{bound} by $V_{\text{weak}} + V_{\text{Coulomb}}$. On the other hand, the wave functions with $V_{\text{HAL}} + V_{\text{Coulomb}}$ and $V_{\text{strong}} + V_{\text{Coulomb}}$ are mostly localized in the range of the folding potential (~ 5 fm). This implies that the Coulomb (strong) interaction gives dominant contribution to form the bound state of $V_{\text{weak}} + V_{\text{Coulomb}}$ ($V_{\text{HAL}} + V_{\text{Coulomb}}$ and

$V_{\text{strong}} + V_{\text{Coulomb}})$.

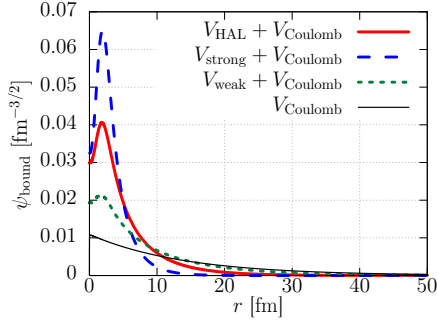


FIG. 7. The bound state wave functions with $V_{\text{HAL}} + V_{\text{Coulomb}}$ (solid line), $V_{\text{strong}} + V_{\text{Coulomb}}$ (dashed line), and $V_{\text{weak}} + V_{\text{Coulomb}}$ (dotted line). For comparison, the bound state wave function with the pure Coulomb case is plotted with thin solid line.

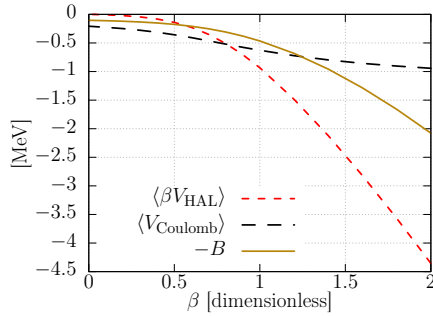


FIG. 8. The β dependence of the expectation values of βV_{HAL} (dashed line), V_{Coulomb} (long-dashed line), and the eigenenergy $-B$ (solid line). The models of $V_{\text{HAL}} + V_{\text{Coulomb}}$, $V_{\text{strong}} + V_{\text{Coulomb}}$, and $V_{\text{weak}} + V_{\text{Coulomb}}$ correspond to the cases with $\beta = 1, 2$, and 0.5 , respectively.

In order to discuss the contribution of the Coulomb potential more quantitatively, we evaluate the expectation values of the folding potential by the strong interaction and of the Coulomb potential. To see the dependence on the strength of the strong interaction, we examine the potential $V(\beta, r)$ by introducing the strength parameter β

$$V(\beta, r) = \beta V_{\text{HAL}}(r) + V_{\text{Coulomb}}(r). \quad (\text{A1})$$

The potential models of $V_{\text{HAL}} + V_{\text{Coulomb}}$, $V_{\text{strong}} + V_{\text{Coulomb}}$, and $V_{\text{weak}} + V_{\text{Coulomb}}$ correspond to the cases with $\beta = 1, 2$, and 0.5 , respectively. In Fig. 8, we show the expectation values of the potentials

$$\langle \beta V_{\text{HAL}} \rangle = \int d^3r |\psi_{\text{bound}}(r)|^2 \beta V_{\text{HAL}}(r), \quad (\text{A2})$$

$$\langle V_{\text{Coulomb}} \rangle = \int d^3r |\psi_{\text{bound}}(r)|^2 V_{\text{Coulomb}}(r), \quad (\text{A3})$$

and the eigenenergy $-B$,

$$-B = \int d^3r [\psi_{\text{bound}}(r)]^* \left[\frac{-\nabla^2}{2\mu_{\Xi^- \alpha}} + V(\beta; r) \right] \psi_{\text{bound}}(r), \quad (\text{A4})$$

with the wave function $\psi_{\text{bound}}(r)$ obtained by $V(\beta, r)$. Note that the eigenenergy $-B$ is given by the sum of the two expectation values of the potentials $\langle \beta V_{\text{HAL}} \rangle + \langle V_{\text{Coulomb}} \rangle$ and the kinetic energy. As we increase β , the binding energy B and the magnitude of the expectation values of the potentials become larger. For $\beta \lesssim 0.8$, $|\langle \beta V_{\text{HAL}} \rangle|$ is smaller than $|\langle V_{\text{Coulomb}} \rangle|$, indicating that the Coulomb potential gives the dominant contribution to the formation of the bound state. For $\beta \gtrsim 0.8$, the contribution of the strong interaction is larger than that of the Coulomb interaction ($|\langle \beta V_{\text{HAL}} \rangle| > |\langle V_{\text{Coulomb}} \rangle|$), because of the stronger β dependence of $\langle \beta V_{\text{HAL}} \rangle$ than $\langle V_{\text{Coulomb}} \rangle$. Thus, these results again suggest that $\Xi^- \alpha$ bound state with V_{weak} ($\beta = 0.5$) originates in the Coulomb interaction, while the bound states with V_{HAL} and V_{strong} ($\beta = 1$ and 2) originate in the strong interaction.

-
- [1] R. L. Jaffe, Phys. Rev. Lett. **38**, 195 (1977), [Erratum: Phys.Rev.Lett. 38, 617 (1977)].
 - [2] K. Nakazawa *et al.*, PTEP **2015**, 033D02 (2015).
 - [3] S. H. Hayakawa *et al.* (J-PARC E07), Phys. Rev. Lett. **126**, 062501 (2021), arXiv:2010.14317 [nucl-ex].
 - [4] M. Yoshimoto *et al.*, PTEP **2021**, 073D02 (2021), arXiv:2103.08793 [nucl-ex].
 - [5] J. Haidenbauer, U.-G. Meißner, and S. Petschauer, Nucl. Phys. A **954**, 273 (2016), arXiv:1511.05859 [nucl-th].
 - [6] K.-W. Li, T. Hyodo, and L.-S. Geng, Phys. Rev. C **98**, 065203 (2018), arXiv:1809.03199 [nucl-th].
 - [7] J. Haidenbauer and U. G. Meißner, Eur. Phys. J. A **55**, 23 (2019), arXiv:1810.04883 [nucl-th].
 - [8] K. Sasaki *et al.*, PoS LATTICE2016, 116 (2017), arXiv:1702.06241 [hep-lat].
 - [9] K. Sasaki *et al.* (HAL QCD), Nucl. Phys. A **998**, 121737 (2020), arXiv:1912.08630 [hep-lat].
 - [10] H. Garcilazo and A. Valcarce, Phys. Rev. C **93**, 034001 (2016), arXiv:1605.04108 [hep-ph].
 - [11] I. Filikhin, V. M. Suslov, and B. Vlahovic, Math. Model. Geom. **5**, 1 (2017), arXiv:1705.03446 [nucl-th].
 - [12] E. Hiyama, K. Sasaki, T. Miyamoto, T. Doi, T. Hatsuda, Y. Yamamoto, and T. A. Rijken, Phys. Rev. Lett. **124**, 092501 (2020), arXiv:1910.02864 [nucl-th].
 - [13] H. Le, J. Haidenbauer, U.-G. Meißner, and A. Nogga, Eur. Phys. J. A **57**, 339 (2021), arXiv:2109.06648 [nucl-th].
 - [14] K. Miyagawa and M. Kohno, Few Body Syst. **62**, 65 (2021), arXiv:2105.11258 [nucl-th].
 - [15] E. Friedman and A. Gal, Phys. Lett. B **820**, 136555 (2021), arXiv:2104.00421 [nucl-th].

- [16] E. Hiyama, M. Isaka, T. Doi, and T. Hatsuda, *Phys. Rev. C* **106**, 064318 (2022), arXiv:2209.06711 [nucl-th].
- [17] E. Friedman and A. Gal, *Phys. Lett. B* **837**, 137640 (2023), arXiv:2209.01606 [nucl-th].
- [18] J. Adams *et al.* (STAR), *Phys. Rev. C* **74**, 064906 (2006), arXiv:nucl-ex/0511003.
- [19] S. Acharya *et al.* (ALICE), *Phys. Rev. C* **99**, 024001 (2019), arXiv:1805.12455 [nucl-ex].
- [20] S. Acharya *et al.* (ALICE), *Phys. Lett. B* **833**, 137272 (2022), arXiv:2104.04427 [nucl-ex].
- [21] S. Acharya *et al.* (ALICE), *Phys. Lett. B* **805**, 135419 (2020), arXiv:1910.14407 [nucl-ex].
- [22] S. Acharya *et al.* (ALICE), *Phys. Rev. Lett.* **123**, 112002 (2019), arXiv:1904.12198 [nucl-ex].
- [23] A. Collaboration *et al.* (ALICE), *Nature* **588**, 232 (2020), [Erratum: *Nature* 590, E13 (2021)], arXiv:2005.11495 [nucl-ex].
- [24] M. Isshiki (STAR), *EPJ Web Conf.* **259**, 11015 (2022), arXiv:2109.10953 [nucl-ex].
- [25] L. Adamczyk *et al.* (STAR), *Phys. Rev. Lett.* **114**, 022301 (2015), arXiv:1408.4360 [nucl-ex].
- [26] S. Acharya *et al.* (ALICE), *Phys. Lett. B* **797**, 134822 (2019), arXiv:1905.07209 [nucl-ex].
- [27] S. Acharya *et al.* (ALICE), *Phys. Lett. B* **844**, 137223 (2023), arXiv:2204.10258 [nucl-ex].
- [28] J. Adam *et al.* (STAR), *Phys. Lett. B* **790**, 490 (2019), arXiv:1808.02511 [hep-ex].
- [29] J. Haidenbauer, *Nucl. Phys. A* **981**, 1 (2019), arXiv:1808.05049 [hep-ph].
- [30] Y. Kamiya, K. Sasaki, T. Fukui, T. Hyodo, K. Morita, K. Ogata, A. Ohnishi, and T. Hatsuda, *Phys. Rev. C* **105**, 014915 (2022), arXiv:2108.09644 [hep-ph].
- [31] J. Haidenbauer and U.-G. Meißner, *PoS CD2021*, 085 (2024), arXiv:2201.08238 [nucl-th].
- [32] J. Haidenbauer and U.-G. Meißner, *EPJ Web Conf.* **271**, 05001 (2022), arXiv:2208.13542 [nucl-th].
- [33] S. Mrówczyński and P. Słoń, *Acta Phys. Polon. B* **51**, 1739 (2020), arXiv:1904.08320 [nucl-th].
- [34] S. Bazak and S. Mrowczynski, *Eur. Phys. J. A* **56**, 193 (2020), arXiv:2001.11351 [nucl-th].
- [35] S. Mrówczyński and P. Słoń, *Phys. Rev. C* **104**, 024909 (2021), arXiv:2103.15761 [nucl-th].
- [36] J. Haidenbauer, *Phys. Rev. C* **102**, 034001 (2020), arXiv:2005.05012 [nucl-th].
- [37] K. Ogata, T. Fukui, Y. Kamiya, and A. Ohnishi, *Phys. Rev. C* **103**, 065205 (2021), arXiv:2103.00100 [nucl-th].
- [38] M. Viviani, S. König, A. Kievsky, L. E. Marcucci, B. Singh, and O. Vázquez Doce, *Phys. Rev. C* **108**, 064002 (2023), arXiv:2306.02478 [nucl-th].
- [39] A. Jinno, Y. Kamiya, T. Hyodo, and A. Ohnishi, *Phys. Rev. C* **110**, 014001 (2024), arXiv:2403.09126 [nucl-th].
- [40] M. Kohno and H. Kamada, (2024), arXiv:2406.13899 [nucl-th].
- [41] B. Singh, *PoS EPS-HEP2021*, 391 (2022).
- [42] Y. Hu (STAR), in *30th International Conference on Ultrarelativistic Nucleus-Nucleus Collisions* (2023) arXiv:2401.00319 [nucl-ex].
- [43] K. Morita, S. Gongyo, T. Hatsuda, T. Hyodo, Y. Kamiya, and A. Ohnishi, *Phys. Rev. C* **101**, 015201 (2020), arXiv:1908.05414 [nucl-th].
- [44] Y. Kamiya and T. Hyodo, *Phys. Rev. C* **93**, 035203 (2016), arXiv:1509.00146 [hep-ph].
- [45] E. Braaten and H. W. Hammer, *Phys. Rept.* **428**, 259 (2006), arXiv:cond-mat/0410417.
- [46] S. E. Koonin, *Phys. Lett. B* **70**, 43 (1977).
- [47] S. Pratt, *Phys. Rev. D* **33**, 1314 (1986).
- [48] S. Pratt, T. Csorgo, and J. Zimanyi, *Phys. Rev. C* **42**, 2646 (1990).
- [49] S. Cho *et al.* (ExHIC), *Prog. Part. Nucl. Phys.* **95**, 279 (2017), arXiv:1702.00486 [nucl-th].
- [50] Y. Kamiya, T. Hyodo, K. Morita, A. Ohnishi, and W. Weise, *Phys. Rev. Lett.* **124**, 132501 (2020), arXiv:1911.01041 [nucl-th].
- [51] J. J. Krauth *et al.*, *Nature* **589**, 527 (2021).
- [52] D. L. Mihaylov, V. Mantovani Sarti, O. W. Arnold, L. Fabbietti, B. Hohlweger, and A. M. Mathis, *Eur. Phys. J. C* **78**, 394 (2018), arXiv:1802.08481 [hep-ph].
- [53] K. Morita, A. Ohnishi, F. Etminan, and T. Hatsuda, *Phys. Rev. C* **94**, 031901 (2016), [Erratum: *Phys. Rev. C* 100, 069902 (2019)], arXiv:1605.06765 [hep-ph].
- [54] R. Lednicky and V. L. Lyuboshits, *Yad. Fiz.* **35**, 1316 (1981).
- [55] A. Andronic, P. Braun-Munzinger, J. Stachel, and H. Stocker, *Phys. Lett. B* **697**, 203 (2011), arXiv:1010.2995 [nucl-th].
- [56] K. Ozawa *et al.*, *EPJ Web Conf.* **271**, 11004 (2022).
- [57] T. Ablyazimov *et al.* (CBM), *Eur. Phys. J. A* **53**, 60 (2017), arXiv:1607.01487 [nucl-ex].